Singlet and Triplet Reaction Paths for Gas-Phase $Zr + C_2H_4$ by Density Functional Theory

Meredith Porembski and James C. Weisshaar*

Department of Chemistry, 1101 University Avenue, University of Wisconsin−Madison, Madison, Wisconsin 53706-1396

Received: January 19, 2001; In Final Form: March 23, 2001

We use the B3LYP density functional theory with a large basis set to characterize stationary points on both triplet and singlet potential energy surfaces for the gas-phase reaction $Zr + C_2H_4 \rightarrow ZrC_2H_2 + H_2$. The previously described stepwise rearrangement path occurs on the triplet surface, requiring passage over a substantial exit channel barrier. A new, lower energy triplet path involves concerted rearrangement of the $HZrC_2H_3$ insertion intermediate directly to a weakly bound, product-like complex with no exit channel barrier to triplet products. A new low-energy singlet path involves stepwise rearrangement from $HZrC_2H_3$ to the strongly bound dihydrido species $H_2ZrC_2H_2$, which then dissociates to singlet products over a small exit channel barrier of 4 kcal/mol. We argue that the singlet path is more consistent than either triplet path with the experimental product kinetic energy distribution, which peaks at 3−5 kcal/mol. This in turn suggests that access of the singlet surface via fast intersystem crossing from the triplet to singlet metallacyclopropane complex competes effectively, perhaps dominating at low collision energy. As in earlier work, B3LYP places key transition state energies too high by 6−9 kcal/mol. The *m*PW1PW91 density functional gives much more realistic energies.

I. Introduction

Several recent studies have established the combination of experiment and electronic structure theory as a powerful approach to elucidation of reaction mechanisms of bare, gas-phase transition metal atoms with hydrocarbons.[1−5] The well-studied metal cation reactions of Fe^+, Co^+, and Ni^+ with ethane, propane, and *n*-butane[1,2,5−8] have served as benchmarks to test the ability of density functional theory to accurately describe key transition state energies in such electronically complex organometallic systems. The popular hybrid density functional B3LYP[9] has led to a comprehensive mechanistic picture of these CC and CH bond activation processes. Careful comparison to all the available experimental data, aided by statistical rate modeling, suggests that B3LYP typically overestimates rate-determining transition states by 5−7 kcal/mol. Nonetheless, it is well established that B3LYP captures the essential features of the potential energy surface (PES) that govern transition metal cation chemistry with much less effort than computationally demanding multireference configuration interaction approaches such as CCSD(T) theory.[10,11]

By comparison, neutral transition metal atom chemistry has been less extensively explored, although the body of experimental and theoretical data is expanding, particularly for the early second-row transition metals Y, Zr, and Nb.[12,13] We have studied the chemical kinetics of Zr ($4d^25s^2$, ^3F) with ethylene and propylene at 300 K using a fast flow reactor equipped with detection by photoionization mass spectrometry (PIMS) at 157 nm.[14,4] Davis and co-workers have studied the chemical dynamics of the $Zr + C_2H_4$ reaction, using a crossed-beam apparatus and PIMS detection at 157 nm at higher collision energies (6−23 kcal/mol).[15] In the past decade, Siegbahn, Blomberg, and others have established a theoretical picture of the interaction of second-row transition metals with small alkenes.[13,16−18] The experimental and theoretical studies agree that the dominant $Zr + C_2H_4$ reaction path involves bimolecular elimination of H_2 from the alkene, although detailed mechanistic questions remain.

The presumption thus far has been that the Zr ($4d^25s^2$, ^3F) + ethylene reaction proceeds exclusively on the triplet PES.[13] Primary CH bond insertion is well understood, proceeding by the formation of a long-lived metallacyclopropane complex, followed by metal insertion into a CH bond of ethylene. Most recently, the absence of a kinetic isotope effect for the $Zr + C_2D_4$ reaction combined with statistical rate modeling revealed that CH bond insertion by the Zr atom must be a facile step that does not control the overall reaction efficiency.[4] Instead, the rate-determining step is initial formation of the strongly bound ZrC_2H_4 complex. This may be inefficient either due to a small approach barrier or nonadiabatic effects in the entrance channel. In contrast, subsequent steps in the mechanism of H_2 elimination from the CH insertion intermediate $HZrC_2H_3$ are not well characterized. Theory indicates that a low-energy stepwise path exists, involving β-hydrogen transfer to form a strongly bound dihydrido intermediate $H_2ZrC_2H_2$.[13]

To date, no study has explicitly confirmed the stepwise mechanism, investigated the possible existence of an exit channel barrier to H_2 elimination, or considered the possible role of the lowest singlet PES in the Zr + ethylene reaction. This paper presents such a detailed theoretical study at the level of B3LYP density functional theory using a large basis set, including complete characterization of all intermediates and transition state structures along both the triplet and singlet potential energy surfaces. Because many studies have found that B3LYP overestimates key barrier heights, we compare the ability of two other hybrid DFT methods, *m*PW1PW91[19,20] and B1LYP,[19] to provide accurate stationary point energies. We find that the triplet PES branches from the insertion intermediate

* Author to whom correspondence should be addressed. E-mail: weisshaar@chem.wisc.edu.

10.1021/jp010219f CCC: $20.00
Published on Web 05/02/2001

TABLE 1: Calculated Energies (kcal/mol) of Stationary Points along the Triplet PES[a]

species	MCPF+ PCI-80[b]	UB3LYP/ Stuttgart+ 6-311++G(d,p)	U*m*PW1PW91/ Stuttgart+ 6-311++G(d,p)[c]	UB1LYP/ Stuttgart+ 6-311++G(d,p)[c]
^{3}**TS$_{ent}$**		+0.78 (+0.68)	−2.2	+1.2
$Zr-C_2H_4$ ($^3B_1$) (**1a**)		−9.7 (−9.9)		
ZrC_2H_4 ($^3A_2$) (**1b**)	−38.0	−28.2 (−28.0)	−38.9	−25.0
^{3}**TS$_{ins}$**	+1.8	+1.9 (+3.1)	−6.2	+5.6
nonplanar $HZrC_2H_3$	−28.7	−27.4 (−26.3)	−33.1	−25.2
planar $HZrC_2H_3$ (**2b**)		−31.6 (−30.4)	−38.3	−29.2
^{3}**TS$_{\beta H}$**	−27.5[d]	−9.8 (−7.5)	−16.0	−6.4
^{3}**MCTS**		−13.7 (−12.1)	−24.4	−9.5
$H_2Zr-C_2H_2$ (**3a**)	−64.0[d]	−18.2 (−15.8)	−22.2	−15.5
$H_2-ZrC_2H_2$ (**3b**)		−15.7 (−14.3)	−24.6	−11.9
^{3}**TS$_{exit}$**		+3.0 (+5.6)	−2.7	+7.2
$Zr-C_2H_2$ ($^3B_1$) + H_2 (**4a**)		+22.0 (+24.4)		
ZrC_2H_2 ($^3A_2$) + H_2 (**4b**)	−18.5	−14.9 (−12.7)	−21.8	−11.6
ZrH_2 ($^3B_1$) + C_2H_2	+18.7[e]	+13.0 (+15.7)		

[a] Energies relative to free reactants, corrected for differential zero-point energy effects; parentheses denote energetics for Zr + C_2D_4. [b] MCPF+PCI-80 calculations by Blomberg and Siegbahn from ref 13, unless otherwise indicated. [c] Single-point energies for all structures optimized at the level of UB3LYP/Stuttgart 6-311++G(d,p). [d] Although the geometry and spin state of these species were not described in ref 13, the energies most likely refer to intermediates along the singlet spin surface (compare to ^{1}**TS$_{\beta H}$** and **7** in Table 3; see text for details). [e] Estimated exothermicity using the heat of formation of C_2H_2 and the calculated binding energy of ZrH_2 ($^3B_1$) from Siegbahn, P. E. M. *Theor. Chim. Acta* **1994**, *87*, 441.

$HZrC_2H_3$ into two low-lying paths. The higher energy, stepwise rearrangement path passes through a dihydrido intermediate and over a substantial exit barrier ^{3}**TS$_{exit}$**, lying 18 kcal/mol above triplet products. The lower energy path directly connects $HZrC_2H_3$ to a product-like complex $H_2-ZrC_2H_2$ via a multicenter transition state ^{3}**MCTS**. In this concerted rearrangement mechanism, the product-like complex smoothly dissociates to ZrC_2H_2 ($^3A_2$) + H_2 products with little or no barrier.

On the singlet PES, all transition states associated with primary CH insertion and stepwise H_2 elimination are lower than the analogous triplet transition states due to the greater bonding capacity of singlet-coupled Zr. We find strong evidence of a low-energy, stepwise path from the singlet metallacyclopropane complex to the exothermic ZrC_2H_2 ($^1A_1$) + H_2 products over a small 4 kcal/mol exit channel barrier ^{1}**TS$_{exit}$**. The singlet path thus stands in significantly better qualitative agreement than either of the low-energy triplet paths with the peaking of the experimental product kinetic energy distribution at 3−5 kcal/mol.[15] Accordingly, we argue that intersystem crossing from the triplet to singlet metallacyclopropane is likely to be important, especially at low collision energy and for small impact parameters. Finally, it appears that the *m*PW1PW91 density functional provides much more accurate transition state energies in these systems than the B3LYP functional.

Throughout this paper, E denotes total energy in the reaction complex, E_t denotes translational energy of reactants, and E_t' denotes translational energy of ZrC_2H_2 + H_2 products. Unless otherwise indicated, all energies of stationary points are reported relative to ground-state Zr ($4d^25s^2$, ^3F) + C_2H_4 reactants, including corrections for zero-point energy (ZPE) effects.

II. Methods

The present work compares most directly to a series of theoretical studies by Siegbahn and others.[16−18] They describe the geometries of potential minima and transition states for the Zr + C_2H_4 reaction optimized at the Hartree−Fock (HF) level and energies at the modified coupled pair functional (MCPF) level. Geometry optimizations used double-ζ (DZ) quality basis sets, while larger sets including diffuse and polarization functions on Zr were used for energy calculations. Later work[13] repeats these calculations, but corrects the MCPF energies using the PCI-80 approximation (Table 1). In the latter study, structural parameters and the spin identity of reaction intermediates were not described. The most recent effort[4] revisits some features of the Zr + ethylene PES, optimizing geometries and computing energies using B3LYP/LANL2DZ (Los Alamos effective core potential (ECP) + DZ valence set for Zr and full DZ set for C and H). When possible, species calculated at the current level of theory will be explicitly compared to structures from these earlier studies.

For geometry optimizations of stationary points, potential energy surface scans, and intrinsic reaction coordinate (IRC) searches from computed transition states, we combine the B3LYP density functional[9] with the Stuttgart ECP + valence set[21] (triple-ζ quality) for Zr and the 6-311++G(d,p) basis set for C and H. We call this hybrid set Stuttgart+6-311++G(d,p) and carry out the electronic structure calculations using the GAUSSIAN-98 (G98) program, either at the spin-restricted (R) or spin-unrestricted (U) level (described further below).[22] The basis set used in this study, while considerably larger than in our previous work (LANL2DZ), does not employ *f* functions on the metal center. However, for this system, the structural and energetic parameters predicted by both LANL2DZ and Stuttgart+6-311++G(d,p) are in good agreement with the calculations using polarized functions at a higher level of theory.[13] In addition, many reviews have noted that DFT methods are not overly sensitive to the size and quality of basis sets.[10,11]

After optimization at the level of UB3LYP/Stuttgart+6-311++G(d,p), we compute single-point energies for most triplet stationary points using two other DFT methods, U*m*PW1PW91 and UB1LYP. Single-point energies for RB3LYP optimized singlet stationary points were also obtained using R*m*PW1PW91. As a test case, we reoptimized the ZrC_2H_4 ($^3A_2$) complex at the level of U*m*PW1PW91/Stuttgart+6-311++G(d,p), but found that the energy decreased by only 0.1 kcal/mol; the geometry and vibrational frequencies remain essentially unchanged. Thus, energies calculated for nonoptimized structures with the different functionals are likely to be realistic. This is consistent with the experience that structural parameters predicted by B3LYP, even with modest basis sets, are of very good accuracy and, unlike energies, geometries and vibrational frequencies tend to be insensitive to the choice of functional employed.[10,11] In a few cases on the triplet PES, a transition state found at the level of UB3LYP/Stuttgart+6-311++G(d,p) actually disappears using the other DFT methods and energies are calculated to lie below the reactant ground-state asymptote, resulting in reported "barrier

heights" below zero. Nonetheless, we report such energies because they are characteristic of the bond-breaking, bond-forming processes with structures the same as the saddle points found with UB3LYP/Stuttgart+6-311++G(d,p).

Electronic stability tests on all optimized stationary points were performed to ensure that the lowest energy solution to the SCF equations was in fact found; all stationary points were found to be stable with the exception of one (described below). For all transition states, an IRC analysis was performed, following the path of steepest descent in both directions until the geometries unambiguously approached those of the expected minima.

For a thorough treatment of the conceptual framework and the practical and theoretical limitations of approximate density functional theory, we refer the reader to excellent discussions by Koch et al.[23] and other reviews of the method.[24,25] However, we do mention one important point here. Because it is the *N*-electron ground-state *density* and not the *N*-electron *wave function* that is defined in DFT, and because the exact exhange-correlation functional is unknown, it remains unclear how to deal with states that must be simultaneous eigenfunctions of $\hat{L}^2$, $\hat{L}_z$, $\hat{S}^2$, and $\hat{S}_z$ for the case of atoms, or of $\hat{S}^2$ and $\hat{S}_2$ for the case of nonlinear polyatomic molecules. The pragmatic approach has been to extract the corresponding quantum numbers from a *single Slater determinant* built from the spin-restricted Kohn−Sham (KS) orbitals themselves, but this is not always possible. Furthermore, the procedure fails if a state is not well-described by a single Slater determinant.

In particular, the magnitude of reported energy barriers and binding energies depends on the choice of the reference atomic ground state. Open-shell, spin-unrestricted atomic states that correspond to a single Slater determinant with a definite value of *L* have been defined by electronic configurations with integer occupancies of the real *d* orbitals as tabulated by Hay.[26] Accordingly, the calculated reference atomic configuration that corresponds to the ground-state term Zr ($4d^25s^2$, ^{3}F) is $d^1_{z^2}$ $d^1_{x^2-y^2}s^2$. Hay does not list the required occupation for the excited-state term Zr ($4d^35s^1$, ^{3}F), so we use the configuration $d^{1.97}_{xz}$ $d^{0.27}_{z^2}$ $d^{0.75}_{x^2-y^2}s^1$ to represent that atomic state. Unfortunately, because we cannot apply symmetry constraints to atoms using the current G98 package, unphysical mixing of the *d* orbitals can occur, leading to noninteger occupancies of *d* orbitals. Nevertheless, the calculated excitation energies of this configuration are 36, 34, and 37 kcal/mol using UB3LYP, U*m*PW1PW91, and UB1LYP, respectively. The experimental excitation energy from ground-state Zr ($4d^25s^2$, ^{3}F) to Zr ($4d^3$-$5s^1$, ^{3}F) is 33 kcal/mol.[27] The agreement between experiment and theory suggests that the energies of chemically bound species will be reasonable. Because the lowest energy singlet atomic state cannot be represented by a single Slater determinant, we do not compute the excitation energy to the excited-state Zr ($4d^25s^2$, ^{1}D); it is 14 kcal/mol experimentally.[27]

Finally, we note that for open-shell species, the value of $\langle\hat{S}^2\rangle$ can be calculated using the determinant built from the spin-unrestricted KS orbitals and compared to the expected magnitude for the true triplet or singlet wave function.[23] When the spin contamination of the unrestricted determinants is significant, the validity of computed structural and energetic parameters is viewed with suspicion. Here, all open-shell triplet calculations were performed at the spin-unrestricted level and deviations of the $\langle\hat{S}^2\rangle$ expectation values were less than 1% for all optimized structures except two, as noted below. Generally, singlet calculations were performed at both the restricted and unrestricted level. In the cases where the unrestricted determinants exhibit severe spin contamination, the spin-restricted calculations presumably provide an upper bound to the true singlet energy and have the additional property of being eigenfunctions of $\hat{S}^2$. Deviations from a pure singlet or triplet description indicate that the true wave function would be better represented by a more sophisticated multi-configurational scheme, beyond the scope of this study. Restricted-open shell DFT methods for *singlets* are currently unavailable within the G98 package.

III. Results

A. Triplet PES. With the electronic wave function constrained to triplet spin multiplicity, we calculate those features of the Zr + ethylene PES illustrated in Figure 1. Below the energy level diagram, we include the key structures that illustrate the major atomic motions along the computed reaction paths, while the detailed structural parameters of all reaction intermediates are given in Figure 2. Table 1 summarizes the energetics of these species, using the Stuttgart+6-311++G-(d,p) basis set with three different density functional methods. Also in Table 1, we collect results from prior theoretical studies. The individual *s* and *d* gross populations and the natural charge of the Zr metal center, as determined by a natural bond orbital (NBO) analysis,[28] are given in Table 2. Finally, rotational constants and vibrational frequencies of all stationary points calculated at the level UB3LYP/Stuttgart+6-311++G(d,p) are collected in the Supporting Information to this paper.

In our earlier study,[4] we searched for a possible barrier to addition of ground-state Zr ($4d^25s^2$, ^{3}F) to the alkene double bond by scanning the distance *R* between Zr and the midpoint of the CC bond. The UB3LYP/LANL2DZ calculations found neither an approach barrier nor a barrier in the region of the curve-crossing (about 2.4 Å) between the Zr−C_2H_4 ($^3B_1$) long-range complex (**1a**) and the ZrC_2H_4 ($^3A_2$) metallacyclopropane complex (**1b**). These two rather different complexes are described below. At the level of UB3LYP/Stuttgart+ 6-311++G-(d,p), we do find a small barrier of +0.78 kcal/mol to the formation of the long-range complex.

The geometry of the entrance channel transition state ^{3}**TS$_{ent}$** is described in Figure 2. The transition state is located at R = 3.44 Å and there is minimal distortion of ethylene; compare structures **1a** and **1b**. The transition vector, also labeled, shows the relative motion of Zr and ethylene along the reaction coordinate, *R*. The calculated energy of ^{3}**TS$_{ent}$** is +1.4 kcal/mol, but the saddle point was determined to be electronically unstable. A lower energy solution finds that ^{3}**TS$_{ent}$** decreases to +0.78 kcal/mol, as reported in Table 2. It is not expected that the structural parameters or vibrational frequencies of ^{3}**TS$_{ent}$** will change significantly in a reoptimization starting from the stabilized electronic state, and none was performed. The basis set superposition error (BSSE)[29] at R = 3.5 Å was previously found to be quite small, +0.04 kcal/mol. The BSSE at R = 3.44 Å, the location of ^{3}**TS$_{ent}$**, should be equally small.[4] Finally, although the PES in the entrance channel is obviously very flat, ^{3}**TS$_{ent}$** does provide a set of vibrational frequencies and rotational constants for the RRKM model (Section IV-B).

Thus the initial interaction of the metal and alkene leads to the formation of a covalently bound complex over at most a small energy barrier. We find that Zr binds to ethylene in two distinct modes with triplet spin multiplicity. The geometry and energy of Zr−C_2H_4 ($^3B_1$) (**1a**) are described in Figure 2 and Table 1. Because *R* is longer, we designate **1a** the long-range complex, rather than a true metallacyclopropane species. The distortion of ethylene is minimal, as indicated by only a slight puckering of the CH bonds and a short CC bond (1.38 Å). The

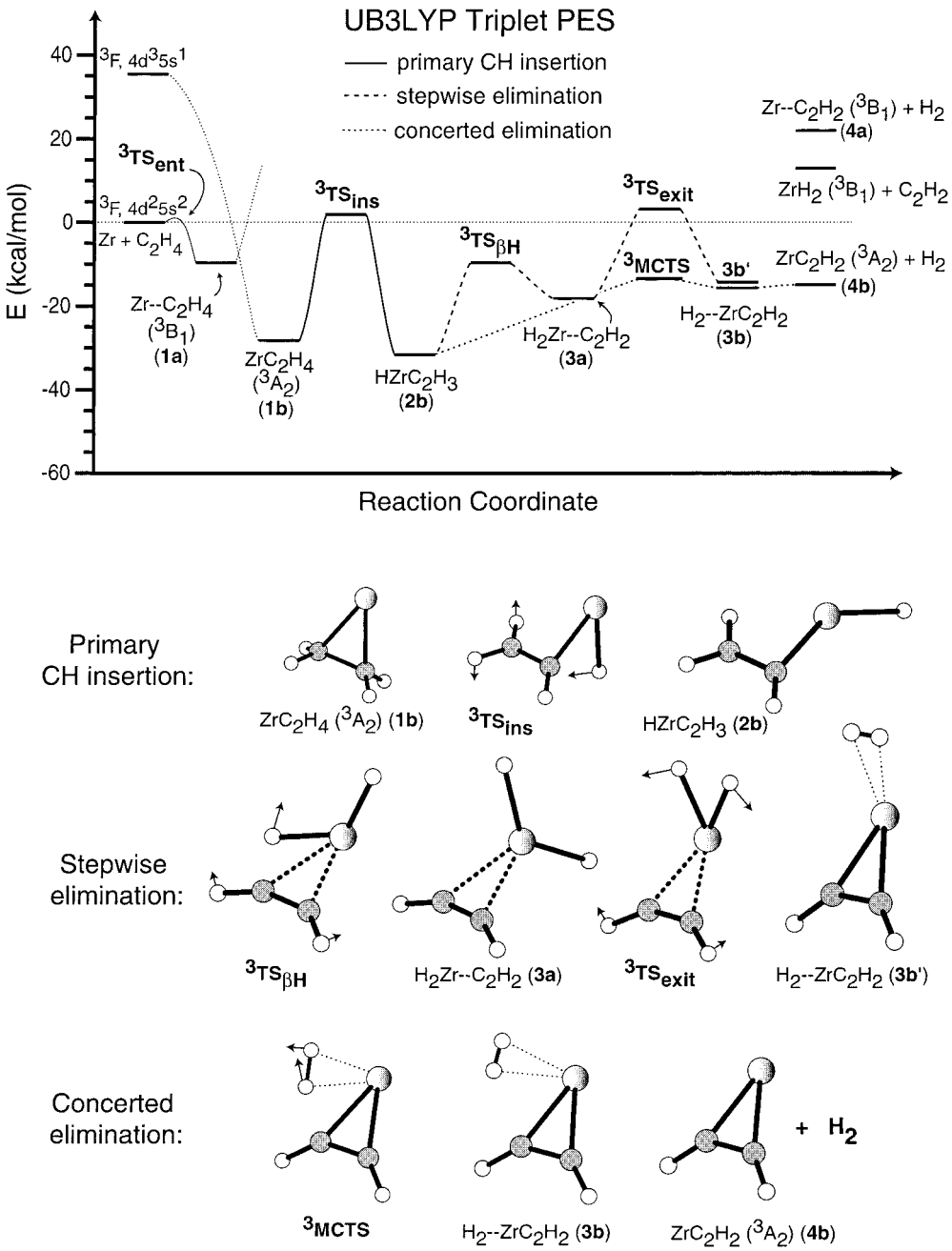

Figure 1. UB3LYP/Stuttgart+6-311++G(d,p) reaction path energetics along the triplet PES. All energies measured relative to ground-state Zr ($4d^25s^2$, ^{3}F) + C_2H_4 reactants and corrected for zero-point energy.

geometry and energy of ZrC_2H_4 ($^3A_2$) (**1b**) are also included in Figure 2 and Table 1. The geometry of this species is nearly identical to the one calculated at the level of UB3LYP/LANL2DZ and to the metallacyclopropane complex calculated at the HF level.[4,16] The binding energy of **1a** is only one-third that of the strongly bound metallacyclopropane and the computed value of $\langle \hat{S}^2 \rangle$ shows a deviation of 9% from a pure triplet spin description. Although a similar long-range complex has been described for Y−C_2H_4, the structure and energy of a long-range, triplet Zr−C_2H_4 complex has not been explicitly reported.[16]

The electron configuration ($d^{2.04}s^{1.62}$) and natural charge (+0.32)[28] of Zr in the long-range complex **1a** reveals that this species retains much of the s^2 character of the ground-state metal atom. In contrast, the metallacyclopropane **1b** exhibits substantial contribution from an excited-state of the metal and a large shift of electron density to the hydrocarbon ($d^{2.31}s^{0.89}$ and natural charge of +0.8). Other calculations have also found the $d^{n-1}s^1$ configuration to be the primary bonding state for early second-row transition metals.[16−18]

The bonding mechanism in the two structurally different complexes follows the discussion outlined by Blomberg et al.,[16] but will be repeated here for clarity. Essentially, to form the two metal−carbon σ bonds of either complex, the d_{yz}, d_{z^2}, and $d_{x^2-y^2}$ metal orbitals (with admixture of only about 12% of the metal *s* orbital) combine to maximize overlap with the p_z orbitals on ethylene. There are six valence electrons to distribute among the ethylene π bond, two Zr−C bonding orbitals, and two metal nonbonding orbitals. In the long-range complex **1a**, the Zr−C bond orbitals are singly occupied and one electron remains in the ethylene π bond; in the metallacyclopropane **1b**, both Zr−C bond orbitals are doubly occupied and the π bond in ethylene is effectively broken. The nonbonding orbitals are another *sd* hybrid orbital (~75% *s*-character) and the d_{xy} orbital, respec-

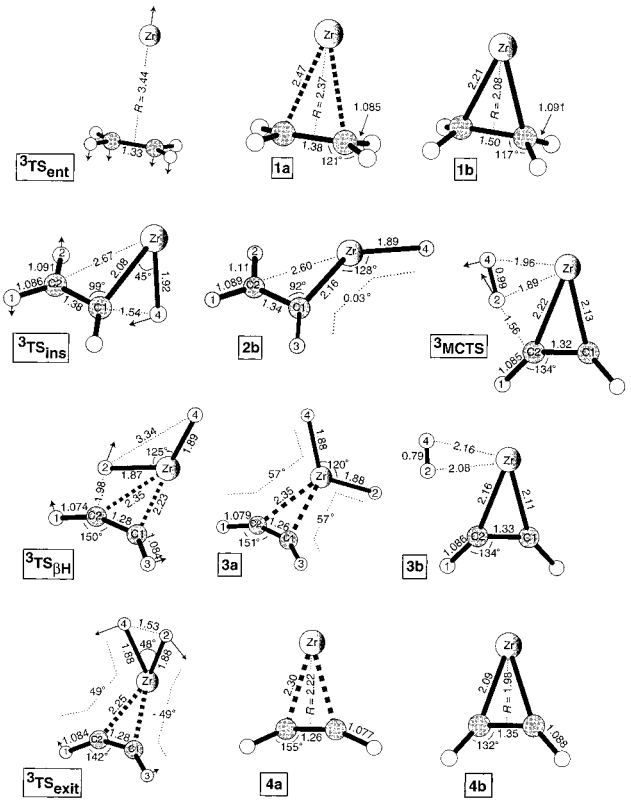

Figure 2. Details of UB3LYP/Stuttgart+6-311++G(d,p) optimized geometries of potential minima and transition states for Zr + C_2H_4 along the triplet PES. Distances in angstroms, angles in degrees. For each transition state, the transition vector corresponding to the imaginary frequency is shown.

TABLE 2: Natural Populations of Zr for Triplet Stationary Points Using UB3LYP/Stuttgart+6-311++G(d,p) Theory

species	natural charge[a]	4d	5s
^{3}**TS$_{ent}$** [b]	+0.01	2.03	1.96
Zr−C_2H_4 ($^3B_1$) (**1a**)	+0.32	2.04	1.62
ZrC_2H_4 ($^3A_2$) (**1b**)	+0.80	2.31	0.89
^{3}**TS$_{ins}$**	+0.62	2.44	0.93
nonplanar $HZrC_2H_3$	+1.01	2.15	0.81
planar $HZrC_2H_3$ (**2b**)	+1.01	2.21	0.76
^{3}**TS$_{\beta H}$**	+1.15	2.20	0.62
^{3}**MCTS**	+0.71	2.50	0.79
$H_2Zr-C_2H_2$ (**3a**)	+1.33	2.07	0.59
$H_2-ZrC_2H_2$ (**3b**)	+0.69	2.51	0.80
^{3}**TS$_{exit}$**	+1.02	2.31	0.63
Zr−C_2H_2 ($^3B_1$) (**4a**)	+0.38	1.57	2.03
ZrC_2H_2 ($^3A_2$) (**4b**)	+0.81	2.30	0.91

[a] The natural charge on Zr, in units of electrons, as found from NBO population analysis; in all cases, the 5p population was less than 0.05. [b] Values listed are for the electronically stable species; see text for details.

tively. Both reduce repulsion with the alkene. In **1a**, the *sd* orbital is doubly occupied. In **1b**, one electron occupies the *sd* orbital, while the second occupies the d_{xy} orbital. Finally, in the long-range complex, the "half-π" bond donates some electron density (0.08 e$^-$) to an empty sd_{z^2} hybrid acceptor orbital.

An essential step toward the elimination of H_2 is insertion into a CH bond of ethylene by the metallacyclopropane complex. The geometry and energy of the triplet CH insertion transition state ^{3}**TS$_{ins}$** that connects the metallacyclopropane (**1b**) to an insertion intermediate (**2b**) are described in Figure 2 and Table 2. The nonplanar structure of ^{3}**TS$_{ins}$** is very similar to the one calculated at the level of UB3LYP/LANL2DZ.[4] Reference 13 reports the energy of a "new and lower" CH insertion transition state than the one previously found (ref 17), but does not describe its geometry. The transition vector for the imaginary frequency, also labeled in Figure 2, clearly indicates the breaking of the CH bond.

The insertion intermediate $HZrC_2H_3$ (**2b**) is described in Figure 2 and Table 1. Most notably, **2b** is planar. Other structural parameters, including the small C2−C1−Zr bond angle, relatively close contact to H2 and the elongation of the β-CH bond are reminiscent of the stabilizing agostic interactions found in many transition metal *cation*-hydrocarbon complexes.[1] A nonplanar insertion intermediate (dihedral angle, $\Theta_{H3-C1-Zr-H4}$ = 128°) was also identified, with structural parameters more similar to the geometry of $HZrC_2H_3$ reported in refs 17 and 4. Its energy is also included in Table 2. Although all DFT methods find the planar $HZrC_2H_3$ (**2b**) to be the global minimum, a potential energy surface scan of the H3−C1−Zr−H4 dihedral angle revealed that a negligible barrier (~1 kcal/mol) separates the two intermediates. Under all reaction conditions, with some 30 kcal/mol of internal energy, rapid conversion between planar and nonplanar $HZrC_2H_3$ will occur. Nonetheless, at the current level of theory, we find **2b** to be the stationary point that is unambiguously connected to ^{3}**TS$_{ins}$** from reactants and to ^{3}**TS$_{\beta H}$** and ^{3}**MCTS** toward products.

After primary CH bond insertion, elimination of H_2 from the insertion intermediate requires transfer of the alkene βH to the metal center. At this level of theory, we find that the triplet PES branches from the planar insertion intermediate **2b**. The large dashed path in Figure 1 follows the stepwise elimination of H_2 via ^{3}**TS$_{\beta H}$**, while the small dashed path follows the concerted elimination of H_2 via ^{3}**MCTS**. The latter is found to be the lowest energy path on the triplet PES to exothermic ZrC_2H_2 ($^3A_2$) + H_2 products.

The βH transfer transition state ^{3}**TS$_{\beta H}$** that carries the planar insertion intermediate (**2b**) to a dihydrido intermediate (**3a**) is described in Figure 2 and Table 1. The labeled transition vector clearly corresponds to the expected β-CH bond stretch. The resulting dihydrido intermediate $H_2Zr-C_2H_2$ (**3a**), distinguished by the formation of strong bonds to hydrogen and weak bonds to acetylene, is described in Figure 2 and Table 1. The geometry and bonding mechanism of the ZrC_2H_2 unit of the complex are virtually identical to the long-range Zr−C_2H_2 ($^3B_1$) complex (**4a**) described below. Furthermore, the geometry of the ZrH_2 unit of the complex is very similar to that calculated for ZrH_2 ($^3B_1$) products (ZrH = 1.87 Å and HZrH = 119°; structure not shown).

However, we find a lower multi-center transition state ^{3}**MCTS** (Table 1) that carries the insertion intermediate (**2b**) *directly* to a product-like complex (**3b**). Figure 2 shows that ^{3}**MCTS** is planar and the structural parameters indicate that the transition state occurs "late" on the potential energy surface. The geometry and bonding mechanism of the ZrC_2H_2 unit are similar to the strongly bound ZrC_2H_2 ($^3A_2$) metallacyclopropene (**4b**) described below. Compared to ^{3}**TS$_{\beta H}$**, the ZrH distances are slightly longer, 1.96 and 1.89 Å, and the H4−H2 distance is much smaller, 0.99 Å. The NBO analysis shows donation of σ_{HH} electron density (0.22 e$^-$) into an empty $sd_{x^2-y^2}$ hybrid orbital on the metal, accompanied by back-donation (0.32 e$^-$) from the Zr−C2 bond to σ_{HH}*. The substantial donor−acceptor interactions among four centers, the two hydrogens, Zr, and C1, inspire us to label this saddle point a multi-center transition state. The transition vector depicted in Figure 2 involving the simultaneous β-CH stretch and formation of molecular H_2,

further reveals the concerted rearrangement of atoms that connects the insertion intermediate directly to the precursor complex for H_2 loss (**3b**). Finally, we note that the geometry at the terminal point of the IRC scan stepping from **^{3}MCTS** toward **2b** is planar, except that the Zr−H4 bond is flipped ($\Theta_{H3C1ZrH4} = 180°$). However, as discussed above, rotation of the Zr−H4 bond is energetically facile.

The resulting $H_2-ZrC_2H_2$ complex (**3b**) is best described as a complex between the metallocyclopropene ZrC_2H_2 and molecular H_2 (Figure 2 and Table 1). Compared to the dihydrido intermediate **3a**, planar **3b** is very product-like. Again, the ZrC_2H_2 unit of the complex is virtually identical to the ZrC_2H_2 ($^3A_2$) complex (**4b**) described below. The ZrH distances are long (2.16 and 2.08 Å) and the H4−H2 distance (0.79 Å) is nearly that of the calculated equilibrium bond length of molecular hydrogen, 0.744 Å. The NBO analysis shows that similar donor−acceptor interactions stabilize this complex, as described above for **^{3}MCTS**. Finally, although **3a** and **3b** differ greatly in geometry, their binding energies are nearly the same. Furthermore, it is not surprising that both **^{3}MCTS** and $H_2-ZrC_2H_2$ (**3b**), with similar product-like geometries and bonding mechanisms, lie nearly isoenergetic to the ZrC_2H_2 ($^3A_2$) + H_2 exit channel.

Before discussing the triplet exit channel PES along the two reaction paths, stepwise H_2 elimination and concerted H_2 elimination, we describe the geometry and energetics of the ZrC_2H_2 + H_2 products themselves. As for ethylene, we find that Zr binds to acetylene in two distinct modes. The geometry and energy of the $Zr-C_2H_2$ ($^3B_1$) complex (**4a**) are described in Figure 2 and Table 1. Like the $Zr-C_2H_4$ ($^3B_1$) complex (**1a**), **4a** binds at a long range; the ZrC bonds are longer, 2.30 Å, and the CC bond length of 1.26 Å is close to the calculated triple bond length in acetylene, 1.20 Å. No similar long-range $Zr-C_2H_2$ complex has been reported in the literature. The geometry and energy of the ZrC_2H_2 ($^3A_2$) complex are also described in Figure 2 (**4b**) and Table 1. We call this complex a metallacyclopropene based on its short ZrC bonds (2.09 Å) and long CC bond (1.35 Å); the computed CC bond length in free ethylene is 1.33 Å. The geometry of **4b** is similar to the structure reported earlier,[18] optimized at the HF level. We calculate the binding energy of **4a** to be only 18.3 kcal/mol, and as for the long-range complex **1a**, there is some spin contamination (12%) of the UB3LYP determinant. We compute a binding energy of 55.1 kcal/mol for **4b**, in good agreement with the binding energy of 56.9 kcal/mol calculated at the MCPF level.[18]

The bonding mechanisms in the acetylene complexes parallel those already described for the ethylene complexes. However, as previously noted by Siegbahn, the interaction of the *out-of-plane* π orbitals with the metal *d* orbitals—not present in the metal−ethylene complexes—accounts for the very strong binding energies of the early second row transition metals, Y, Zr, and Nb with acetylene.[18] Essentially, the out-of-plane acetylene π orbital donates electron density into the unoccupied metal d_{xz} orbital accompanied by back-donation of d_{xy} electron density to the π^* orbital.

The exit channel PES for the Zr + ethylene reaction governs the disposal of energy into H_2 elimination products. Thus far, we have shown the existence of a dihydrido intermediate $H_2-Zr-C_2H_2$ (**3a**) and also a bound complex between ZrC_2H_2 and molecular H_2 (**3b**), whose structure is much more like ground-state products. The corresponding rearrangement transition states are **^{3}TS$_{\beta H}$** and **^{3}MCTS**. Next, we directly explore the connection of **3a** and **3b** to products following either the stepwise H_2 elimination reaction path or the concerted H_2 elimination reaction path along the triplet PES.

The geometry and energy of the transition state **^{3}TS$_{exit}$** that connects the dihydrido intermediate $H_2Zr-C_2H_2$ (**3a**) to products are given in Figure 2 and Table 1. To reach the ZrC_2H_2 ($^3A_2$) + H_2 exit channel, **3a** must make a significant geometry change; the transition vectors in Figure 2 involve the H4−Zr−H2 angle bend and reorientation of the acetylene group. The IRC analysis determined that **^{3}TS$_{exit}$** leads directly to another $H_2-ZrC_2H_2$ exit channel complex. This species, whose structure is shown in Figure 1 (**3b′**), appears to be an isomer of **3b**. The donor−acceptor interactions, $\sigma_{HH} \rightarrow d_{xz}$ and $d_{xy} \rightarrow \sigma_{HH}^*$, account for the perpendicular, rather than coplanar, arrangement of H_2. Complex **3b′** is nearly isoenergetic to the ZrC_2H_2 ($^3A_2$) + H_2 exit channel and, based on the H_2 dissociation scan from **3b** (discussed below), we do not expect any further barrier beyond this complex. Thus, we consider **^{3}TS$_{exit}$** to be the effective barrier (∼18 kcal/mol) for formation of the dihydrido intermediate $H_2-Zr-C_2H_2$ (**3a**) from isolated ZrC_2H_2 + H_2 ground-state reactants.

In contrast, we find no exit channel barrier for the concerted elimination of H_2 along the triplet spin surface. Starting from the $H_2-ZrC_2H_2$ (**3b**) minimum, we compute the energy while scanning the distance between Zr and H4, optimizing the geometry at each fixed value of Zr−H4. At the level of UB3LYP/Stuttgart+6-311++G(d,p), we find that **3b** dissociates to ZrC_2H_2 ($^3A_2$) + H_2 products with monotonically increasing energy.

Finally, we note that the three DFT methods predict a wide range of energies for all species along the triplet PES, as shown in Table 1. Compared to the B3LYP calculations, *m*PW1PW91 increases binding energies and lowers transition states relative to ground-state reactants by about 7 kcal/mol on average, while B1LYP decreases binding energies and increases transition states by about 3 kcal/mol on average. We assess the relative performance of the different theories in explaining the behavior of the Zr + ethylene system below.

B. Singlet PES. Analogous calculations for the Zr + ethylene system constrained to singlet spin multiplicity were carried out at the spin-restricted level using the B3LYP density functional (RB3LYP/Stuttgart+6-311++G(d,p)). The results are displayed in Figures 3 and 4 and Tables 3 and 4. In all cases, reoptimization at the spin-unrestricted level (UB3LYP) did not significantly change geometries or vibrational frequencies. For the closed-shell species **^{1}TS$_{ins}$**, $HZrC_2H_3$ (**6**), **^{1}TS$_{\beta H}$**, and $H_2ZrC_2H_2$ (**7**), the RB3LYP and UB3LYP energies were virtually identical. For the species with nonbonding, spin-paired electrons, including ZrC_2H_4 ($^1A_1$) (**5**), **^{1}TS$_{exit}$**, and ZrC_2H_2 ($^1A_1$) (**8**), and for some points along the exit channel PES scan, the UB3LYP calculations significantly lowered energies relative to the RB3LYP values. Substantial spin contamination of the UB3LYP determinants was observed for such structures, as reported in Table 3. In these cases, we view the spin-restricted energies as likely upper bounds to the true singlet surface, as described above. Similar to the triplet PES, the R*m*PW1PW91 calculations yield significantly lower energies compared to the RB3LYP values for most singlet stationary points (Table 3). Finally, rotational constants and vibrational frequencies of all singlet stationary points calculated at the level of RB3LYP/Stuttgart+6-311++G(d,p) are collected in the Supporting Information to this issue.

The singlet mechanism is qualitatively similar to the stepwise triplet mechanism described above. The geometry and energy of the ZrC_2H_4 ($^1A_1$) metallacyclopropane complex (**5**) are given in Figure 4 and Table 3. The electron configuration of Zr

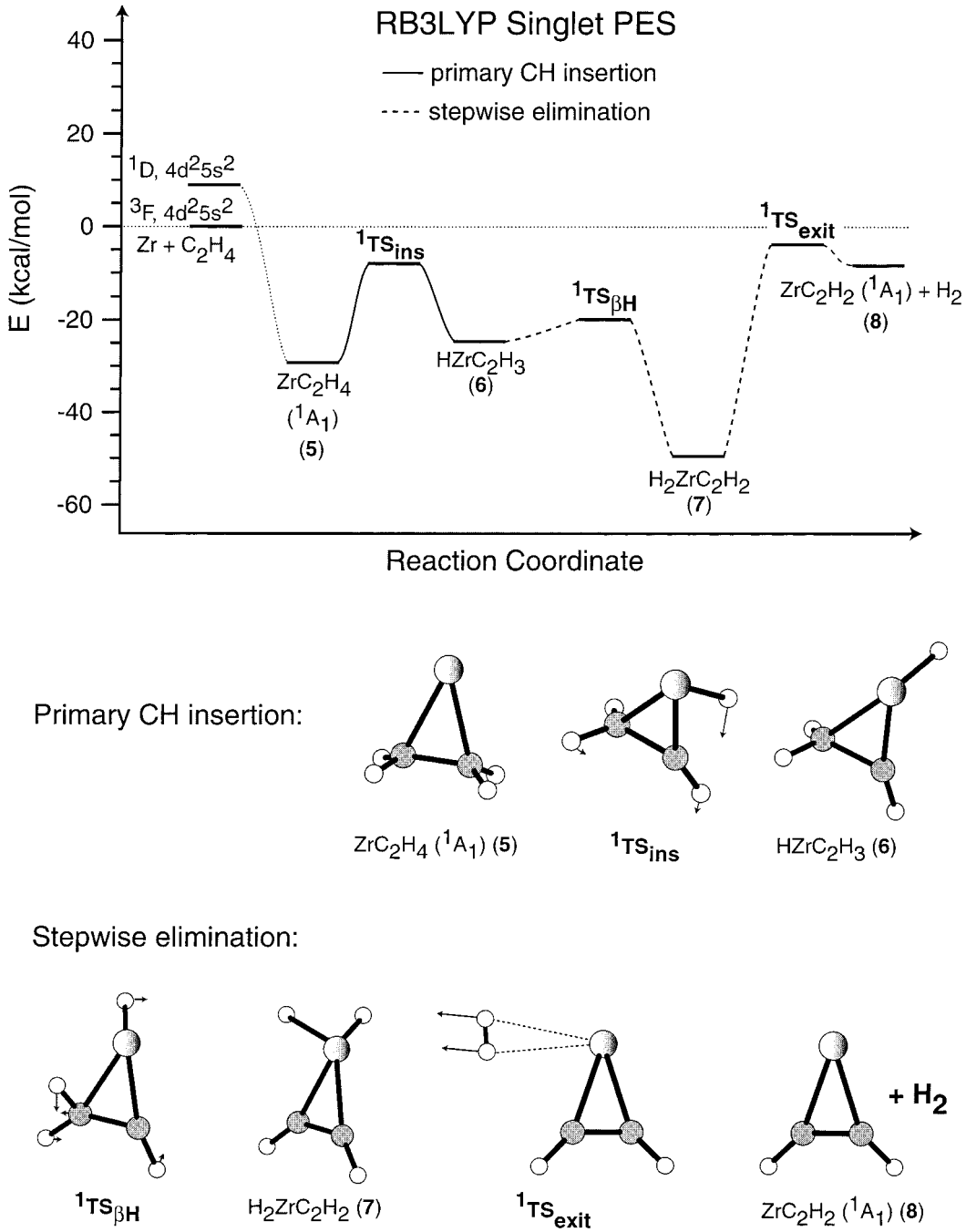

Figure 3. RB3LYP/Stuttgart+6-311++G(d,p) reaction path energetics along the singlet PES. All energies measured relative to ground-state Zr ($4d^25s^2$, ^{3}F) + C_2H_4 reactants and corrected for zero-point energy.

($d^{1.55}s^{1.74}$) indicates a correlation to the $4d^25s^2$, ^{1}D electronic state of the metal (Table 4). The bonding mechanism for **5** follows the description of the ZrC_2H_4 ($^3A_2$) complex (**1b**) outlined above except that the two nonbonding electrons are now spin-paired in an *sd* hybrid orbital that reduces repulsion with ethylene. Not surprisingly, the geometries of the triplet and singlet ZrC_2H_4 complexes are virtually identical.

The geometry and energy of the CH insertion transition state **^{1}TS$_{ins}$** that connects the metallacyclopropane (**5**) to an insertion intermediate (**6**) is described in Figure 4 and Table 3. The structure of **^{1}TS$_{ins}$** is quite different from **^{3}TS$_{ins}$** (Figure 2). The singlet transition state is "late," with the CH bond fully broken and the ZrH bond essentially fully formed. In addition, Zr can use all four electrons to form strong bonds to *both* carbons on ethylene *and* the hydrogen, as indicated by the short Zr−C1, Zr−C2, and Zr−H4 distances. In fact, ZrC1 is a double bond and the CC bond length (1.48 Å) is close to that of free ethane, 1.54 Å. As a result, **^{1}TS$_{ins}$** already has considerable metallacyclopropane character; compare structures **5** and **6**. Accordingly, at the level of RB3LYP/Stuttgart+6-311++G(d,p), **^{1}TS$_{ins}$** lies nearly 10 kcal/mol below **^{3}TS$_{ins}$**. The transition vector indicates the expected CH bond stretch and reorientation of the C1−H3 bond.

The geometry and energy of the singlet insertion intermediate $HZrC_2H_3$ (**6**) are displayed in Figure 4 and Table 3. As in **^{1}TS$_{ins}$**, Zr uses all four electrons to form a double bond to C1 and single bonds to C2 and H4; the structure bears strong similarity to the metallacyclopropane complex (**5**).

In contrast to the triplet PES, we find a single low-energy path to ZrC_2H_2 ($^1A_1$) + H_2 products involving the stepwise elimination of H_2 from the insertion intermediate (**6**). The βH transfer transition state **^{1}TS$_{\beta H}$** that connects **6** to a strongly bound

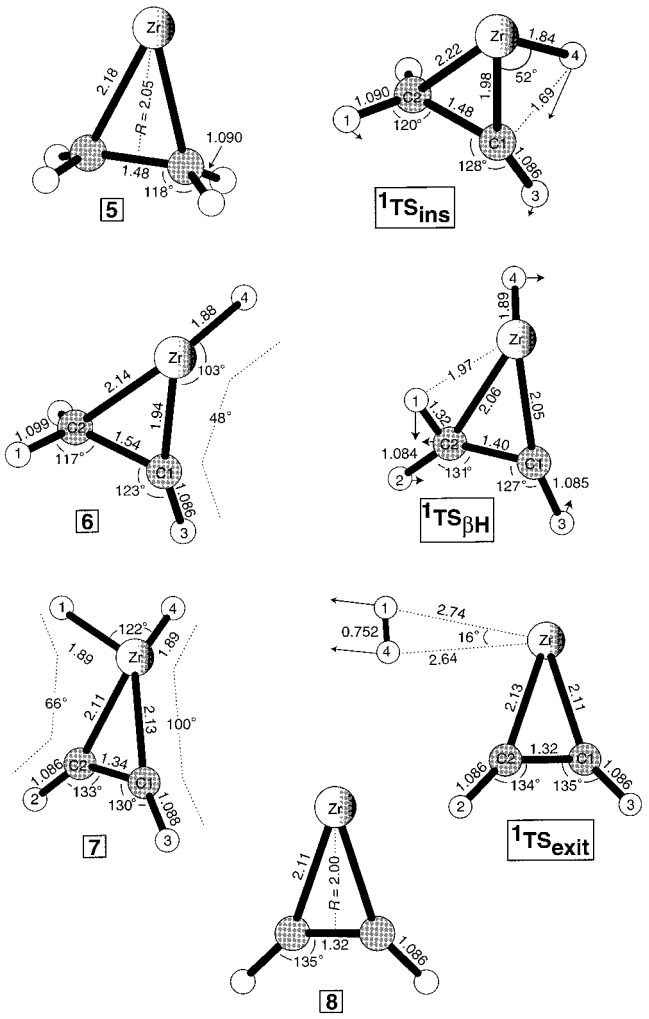

Figure 4. Details of RB3LYP/Stuttgart+6-311++G(d,p) optimized geometries of potential minima and transition states for Zr + C_2H_4 along the singlet PES. Distances in angstroms, angles in degrees. For each transition state, the transition vector corresponding to the imaginary frequency is shown.

TABLE 3: Calculated Energies (kcal/mol) of Stationary Points along the Singlet PES[a]

species	RB3LYP/ Stuttgart+ 6-311++G(d,p)	UB3LYP/ Stuttgart+ 6-311++G(d,p)	$\langle\hat{S}^2\rangle$[b]	R*m*PW1PW91/ Stuttgart+ 6-311++G(d,p)[c]
ZrC_2H_4 ($^1A_1$) (**5**)	−29.3 (−29.1)	−31.2 (−31.0)	0.6	−35.2
^{1}**TS$_{ins}$**	−7.9 (−6.8)	−7.9 (−6.8)	0	−15.3
$HZrC_2H_3$ (**6**)	−24.6 (−22.7)	−24.6 (−23.3)	0	−31.9
^{1}**TS$_{\beta H}$**	−19.9 (−17.9)	−19.9 (−17.9)	0	−27.3
$H_2ZrC_2H_2$ (**7**)	−49.5 (−47.4)	−49.5 (−47.4)	0	−54.3
^{1}**TS$_{exit}$**	−4.3 (−2.5)	−12.2 (−10.2)	0.9	−7.1
ZrC_2H_2 ($^1A_1$) + H_2 (**8**)	−8.3 (−6.1)	−13.9 (−11.6)	0.8	−10.1

[a] Energies relative to ground-state, triplet reactants, Zr ($4d^25s^2$, ^{3}F) + C_2H_4, corrected for differential zero-point energy effects. Parentheses denote energetics for Zr + C_2D_4. [b] Computed average value $\langle\hat{S}^2\rangle$ measures the spin contamination of the UB3LYP determinants. [c] Single-point energies for structures optimized at the level of RB3LYP/ Stuttgart+6-311++G(d,p).

dihydrido intermediate (**7**) is described in Figure 4 and Table 3. Again, it is the simultaneous interaction of Zr in its singlet spin state with C1, C2, H1, and H4 that lowers the energy of ^{1}**TS$_{\beta H}$** relative to ^{3}**TS$_{\beta H}$** by 10 kcal/mol. The NBO analysis identifies β-CH agostic interactions with the metal center that account for the substantial lengthening of the C2−H1 bond (1.32 Å). Furthermore, the transition vector in Figure 4 involves primarily this β-CH bond stretch and also the reorientation of the acetylene group. Neither the structural parameters nor the identity of the spin state of the earlier βH transfer transition state were reported,[13] but its energy is given in Table 1. Comparing the energies of ^{3}**TS$_{\beta H}$** and ^{1}**TS$_{\beta H}$** (Tables 1 and 3) to the PCI-80 calculation suggests that the original transition state was a singlet species.

TABLE 4: Natural Populations of Zr for Singlet Stationary Points Using RB3LYP/Stuttgart+6-311++G(d,p) Theory

species	natural charge[a]	4d	5s
ZrC_2H_4 ($^1A_1$) (**5**)	+0.72	1.55	1.74
^{1}**TS$_{ins}$**	+0.82	1.09	2.11
$HZrC_2H_3$ (**6**)	+1.32	0.44	2.28
^{1}**TS$_{\beta H}$**	+1.19	2.46	0.37
$H_2ZrC_2H_2$ (**7**)	+1.64	1.93	0.45
^{1}**TS$_{exit}$**	+0.69	1.81	1.50
ZrC_2H_2 ($^1A_1$) (**8**)	+0.71	1.59	1.71

[a] The natural charge on Zr in units of electrons, as found from NBO population analysis; in all cases, the 5*p* population was less than 0.01.

The geometry and energy of the $H_2ZrC_2H_2$ complex (**7**) are shown in Figure 4 and Table 3. The singlet dihydrido intermediate (**7**) is more strongly bound than the triplet dihydrido intermediate (**3a**) by over 30 kcal/mol. In contrast to its triplet counterpart, the closed-shell complex can form strong bonds with *both* H_2 and C_2H_2, as revealed by the short ZrH and ZrC bond lengths. The geometry of **7** is distinctly asymmetric, with both hydrogens on the same side of the metal center. At the current level of theory, we find that the analogous structure with C_{2v} symmetry (H_2 axis perpendicular to the ZrC_2H_2 plane) is a saddle point with one imaginary frequency of 89i cm^{-1}, lying less than 1 kcal/mol above the minimum described here. We will find additional evidence of soft hydrogen motion relative to the ZrC_2H_2 frame further along the singlet reaction path. In the earlier study,[13] neither the geometry nor the identity of the spin state of the $H_2ZrC_2H_2$ complex were reported. Nonetheless, based on its binding energy (Table 1), the species was surely the singlet dihydrido intermediate.

Before discussing the elimination of H_2 from the dihydrido intermediate (**7**) in some detail, we describe the ZrC_2H_2 ($^1A_1$) + H_2 products themselves. The geometry and energy of the ZrC_2H_2 ($^1A_1$) complex (**8**) are given in Figure 4 and Table 3. The structure of **8** is virtually identical to the strongly bound triplet metallacyclopropene (**4b**). The binding energy of 48.5 kcal/mol and the calculated reaction exothermicity of −8.3 kcal/mol are also close to the corresponding triplet energies. There is a significant admixture of the Zr ($4d^25s^2$, ^{1}D) electronic state ($d^{1.59}s^{1.71}$, Table 4), and the bonding mechanism follows the description of the triplet metallacyclopropene outlined above except that the two nonbonding electrons are spin-paired in an *sd* hybrid orbital. There is a considerable shift of out-of-plane π electron density (0.19 e^-) into the empty d_{xz} orbital, but no appreciable metal back-donation.

An important mechanistic question is whether a low-energy singlet reaction path leads from the dihydrido intermediate (**7**) to elimination products. Hence, we now describe in detail our investigation of coordinate scans along the singlet exit channel PES. The results are summarized in Figure 5, calculated at the level of RB3LYP/Stuttgart+6-311++G(d,p). The open triangles plot the energy (uncorrected for ZPE) as a function of *decreasing* the H1−Zr−H4 bond angle in $H_2ZrC_2H_2$ (**7**). A geometry optimization is performed at each fixed value of H1−Zr−H4. The energy smoothly increases to +3.4 kcal/mol at H1−Zr−

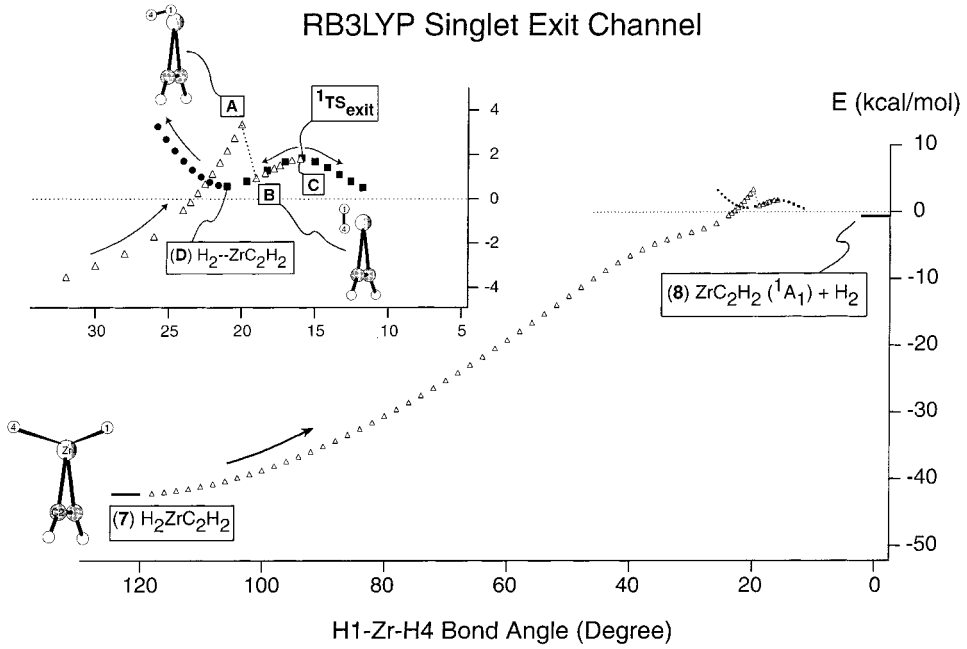

Figure 5. RB3LYP/Stuttgart+6-311++G(d,p) potential energy surface scans of the singlet exit channel connecting $H_2ZrC_2H_2$ (**7**) to ZrC_2H_2 ($^1A_1$) + H_2 products. At each value of angle H1−Zr−H4, all other coordinates are optimized. Energies uncorrected for zero-point effects. Open triangles depict the energy as a function of increasing the H1−Zr−H4 bond angle from **7**. Points **A**, **B**, and **C** in the inset mark points along this scan. Filled squares illustrate the IRC following from ^{1}**TS**$_{exit}$. Point **D** marks the minimum found along this scan. Filled circles depict the energy as a function of decreasing the H1−Zr−H4 bond angle from **D**. See text for details.

H4 = 20° (**A**), abruptly decreases to +0.9 kcal/mol at H1−Zr−H4 = 19° (**B**), and then slowly rises again to a maximum at H1−Zr−H4 = 16° (**C**). These positions are marked in the inset of Figure 5. Accompanying the abrupt change in energy between **A** and **B**, there is but a small change in geometry. In both product-like species, the structural parameters of the ZrC_2H_2 unit are very similar to ZrC_2H_2 ($^1A_1$) (**8**, Figure 2). Furthermore, in **A** (**B**) the Zr−H1 and Zr−H4 distances are 2.18 Å (2.33 Å) and 2.18 Å (2.25 Å), respectively, and the H1−H4 distance is 0.757 Å (0.759 Å). The primary difference is the position of H_2 relative to the ZrC_2H_2 frame. Figure 5 shows views of **A** and **B** with the ZrC_2H_2 unit oriented almost perpendicular to the plane of the paper. **A** is nonplanar, while **B** is planar.

Using the structure at **C** (also planar) as input, a successful transition state optimization was performed. The geometry and energy of ^{1}**TS**$_{exit}$ are shown in Figure 4 and Table 3; its energy uncorrected for ZPE is also indicated in the inset of Figure 5. Again, the planar transition state ^{1}**TS**$_{exit}$ is very product-like. The structural parameters of the ZrC_2H_2 unit are similar to **8**; the Zr−H1 and Zr−H4 distances have increased to 2.74 and 2.64 Å, respectively, and the H1−H4 distance is 0.752 Å. The labeled transition vector depicts motion that clearly leads to elimination products. The filled squares in Figure 5 illustrate the results of the IRC following from ^{1}**TS**$_{exit}$ outward, confirming the connection to the ZrC_2H_2 ($^1A_1$) + H_2 exit channel. In the direction back toward **7**, the IRC scan identifies a shallow minimum at H1−Zr−H4 = 21° (**D**). The structure of that weakly bound H_2−ZrC_2H_2 complex is virtually identical to the triplet H_2−ZrC_2H_2 complex **3b**, described above (Figure 2).

In an attempt to establish the connection of the singlet H_2−ZrC_2H_2 (**D**) complex to the strongly bound dihydrido intermediate $H_2ZrC_2H_2$ (**7**), we performed a potential energy surface scan *increasing* the H1−Zr−H4 angle from the product-like minimum. The filled circles in Figure 5 illustrate those results. We find that the energy rapidly increases, *crossing* that of the previous bond angle scan carried out in the opposite direction (triangles). All the structures represented by the closed circles are planar.

In effect, at this level of theory we have identified two *diabatic* surfaces that intersect in the vicinity of H1−Zr−H4 = 22°. By *diabatic* we mean preserving both electron configuration and spin. An NBO analysis of the Zr population at **A** gives $d^{2.61}s^{0.51}$ and reveals that both the electron configuration of Zr ($d^{1.93}s^{0.45}$) and the nonplanar geometry of $H_2ZrC_2H_2$ (**7**) have been retained along the forward bond angle scan (triangles). In contrast, the points along the IRC scan (squares) and the reverse bond angle scan (circles) have electron configurations that more closely match Zr ($d^{1.71}s^{1.59}$) in ZrC_2H_2 ($^1A_1$) (**8**) and planar geometries. For example, the configurations at H_2−ZrC_2H_2 (**D**) and ^{1}**TS**$_{exit}$ are Zr ($d^{2.00}s^{1.36}$) and Zr ($d^{1.81}s^{1.50}$), respectively. Qualitatively speaking, from the dihydrido intermediate (**7**) toward products, electron density must flow out of the ZrH bonds into a nonbonding orbital. Along the diabatic curve emanating from **7**, the nonbonding electrons evolve to occupy an *sd*-hybrid orbital of mostly *d*-character, while the electrons occupy an *sd*-hybrid of primarily *s*-character along the diabatic curve that correlates to products. Despite the similar geometries near the surface intersection, the energies differ because of the different orbital occupancies. However, along the forward bond angle scan (triangles), the calculations *do* find a lower energy solution to the SCF equations at **B** that directly correlates to the ZrC_2H_2 ($^1A_1$) + H_2 exit channel, involving a change of electron configuration to the d^2s^2-like state of the products.

The RB3LYP calculations are evidently unable to find the *adiabatic* surface that smoothly connects the dihydrido intermediate (**7**) to elimination products. All attempts to find a transition state in the region of the curve-crossing failed, using either wave function as the initial guess. Searches for the adiabatic reaction path involving other reaction coordinates were also unsuccessful. For example, in scans involving the H4−

H1−Zr−C2 dihedral angle of the $H_2-ZrC_2H_2$ complex (**D**) and scans using a radial coordinate (distance from Zr to the midpoint of H_2), we have located another set of geometries that fail to converge near the same surface intersection at essentially the same total energy. As described above, the electron configuration at Zr must change substantially from $H_2ZrC_2H_2$ (**7**) *en route* to products. RB3LYP cannot provide sufficient multiconfigurational character in the vicinity of the diabatic surface intersection to accurately describe the nature of such a transition state.

Our results, however, clearly indicate that there does exist a low-energy singlet path from **7** to products. Because the two diabatic surfaces that intersect are of the same spin, the mixing and splitting at the intersection shown in Figure 5 should be substantial. Furthermore, since the diabatic crossing point already lies *below* ^{1}**TS$_{exit}$**, we expect no additional barrier along the adiabatic surface. Thus, in Figure 3 and our mechanistic discussion below, we consider ^{1}**TS$_{exit}$** to be the effective exit channel barrier to formation of the ZrC_2H_2 ($^1A_1$) + H_2 products from the dihydrido intermediate (**7**) on the singlet PES. Significantly, ^{1}**TS$_{exit}$** lies 4 kcal/mol above product when both are computed at the RB3LYP level. Since the geometry of ^{1}**TS$_{exit}$** is already quite product-like, we expect that a more flexible open-shell singlet treatment of both ^{1}**TS$_{exit}$** and singlet products would preserve this ∼4 kcal/mol barrier.

IV. Discussion

A. Overview of Experimental and Theoretical Results. Chemical kinetics data at 300 K (0.9 kcal/mol mean collision energy) and 0.5−0.8 Torr buffer gas provide the bimolecular rate constant for Zr + C_2H_4, $k_H = 55 \times 10^{-12}$ cm^3 s^{-1}.[12] The reaction efficiency, estimated as k_H/k_{LJ}, is only 7%; here k_{LJ} is the Lennard−Jones rate constant estimated as before.[4] No kinetic isotope effect is observed on perdeuteration; $k_H/k_D = 1.05 \pm 0.05$.[4] Over the limited flow tube pressure range of 0.5−1.1 Torr, PIMS at 157 nm detects only elimination products, ZrC_2H_2 or ZrC_2D_2. Stabilized collision complexes are estimated to contribute no more than 10% of the primary products, based on experimental sensitivity.

Crossed-beam scattering angular distributions provide complementary information on the Zr + C_2H_4 reaction at higher collision energies between 6 and 23 kcal/mol.[15] At 5.9 kcal/mol, the center-of-mass angular distribution of nonreactive Zr atoms is distinctly forward peaked, indicating the absence of backscattered metal atoms from dissociation of long-lived ZrC_2H_4 collision complexes. Evidence of such long-lived complexes is first observed at 9.1 kcal/mol, and becomes substantial at both 14.0 and 23.1 kcal/mol. At all collision energies, ZrC_2H_2 products are detected with forward−backward symmetric center-of-mass angular distributions and kinetic energy distributions $P(E_t')$ that peak distinctly above zero kinetic energy. Such product distributions are consistent with a mechanism that proceeds via intermediates having lifetime greater than a rotational period, and with a modest exit channel barrier above the ZrC_2H_2 + H_2 product asymptote.

The electronic structure calculations of this study reveal many new mechanistic features of the Zr + ethylene reaction. First, the existence of the long-range complexes Zr−C_2H_4 (**1a**) and Zr−C_2H_2 (**4a**) shows that rather than being chemically inert, s^2 metal atoms can form chemical bonds with little or no barrier. For the early transition metals Y and Zr, the fully occupied *s* orbital can hybridize with empty *d* orbitals to effectively reduce electron repulsion toward the hydrocarbon, while maintaining some bonding interaction with the π bond of the alkene or alkyne. As a result, the barrier to the addition of ground-state Zr to the CC bond is no more than 1 kcal/mol. Second, *two* distinct reaction paths on the triplet PES have been found, a stepwise path and a concerted path. Both ultimately lead to exothermic ZrC_2H_2 ($^3A_2$) + H_2 products. Although the quantitative details depend on the density functional employed, all methods predict that the lowest energy path involves the *concerted* elimination of H_2 from the strongly bound insertion intermediate (**2b**) over the multi-center transition state ^{3}**MCTS** with no subsequent exit channel barrier.

Interestingly, for the H_2 elimination mechanisms of Fe^+ ($3d^6$-$4s^1$, ^{6}D), Co^+ ($3d^8$, ^{3}F) and Ni^+ ($3d^9$, ^{2}D) with ethane and propane, B3LYP calculations find that the lowest energy reaction path again involves an MCTS.[1,5−8] Other calculations have predicted the concerted elimination of H_2 via a similar MCTS for the *neutral* transition metal reaction Pt ($5d^96s^1$, ^{3}D) + CH_4.[30] In all such examples, concerted rearrangement to a loosely bound exit-channel complex over a multi-centered transition state is energetically favored over stepwise rearrangement because the metal center lacks sufficient bonding capacity to form covalent bonds to both hydrogen atoms and to the remaining hydrocarbon fragment. Agostic interactions between the metal center and the σ_{CH} bond or the σ_{HH} bond, as found here for ^{3}**MCTS**, evidently play a significant role in the stability of all such transition states.

The new calculations also find a low-energy *singlet* path to exothermic ZrC_2H_2 ($^1A_1$) + H_2 products. All barriers associated with primary CH insertion and stepwise H_2 elimination along the singlet PES lie well below ground-state triplet reactants, due to the ability of Zr in its singlet spin state to form strong covalent bonds. This extra bonding capacity of singlet Zr obviates the need for a MCTS. Therefore, in contrast to the triplet PES, the Zr + ethylene reaction on the singlet PES proceeds via the stepwise mechanism, involving a small exit barrier to the elimination of H_2 from the strongly bound dihydrido intermediate (**7**).

B. Reaction Mechanism. *1. Triplet Path Revisited.* The long-standing view of the Zr + ethylene reaction based on the PCI-80 calculations of Siegbahn et al. (Table 1) involves rate-determining primary CH insertion from the metallacyclopropane complex on the *triplet* spin surface.[13] Other stationary points along the stepwise H_2 elimination path were found to lie well below the energy of reactants, and any exit channel barrier from the strongly bound dihydrido intermediate was anticipated to be small. It is now clear that both the βH transfer transition state and the $H_2ZrC_2H_2$ complex were in fact stationary points along the *singlet* spin surface.

In a more recent study, UB3LYP/LANL2DZ calculations confirmed the mechanism of primary CH insertion along the triplet PES outlined by the earlier theoretical work.[4] Furthermore, using RRKM theory[31,32] based on the UB3LYP/LANL2DZ geometries and frequencies, we modeled the decay of long-lived metallacyclopropane complexes and explored what range of energies of key stationary points yield behavior consistent with experiment. Both the absence of an isotope effect at 300 K[4] and the absence of backscattered Zr at low collision energies[15] indicate that CH insertion by the metallacyclopropane must be facile. Specifically, when ^{3}**TS$_{ins}$** lies at −4 to −7 kcal/mol, essentially all complexes go on to insert into a CH bond of ethylene and eliminate H_2 rather than dissociate back to reactants. Under room-temperature reaction conditions, the rate model predicts that ZrC_2H_4 complexes then live on the order of 1 ns, too short for stabilization by a third-body collision in

the flow tube at 0.5−1.1 Torr. This is consistent with the product branching data from PIMS. At higher collision energy, angular momentum barriers atop ^{3}**TS$_{ins}$** deflect some ZrC_2H_4 complexes back to reactants, as experimentally observed.[15] The kinetics data set an upper bound on ^{3}**TS$_{ins}$**, while the onset of backscattering in turn sets a lower bound on the energy of ^{3}**TS$_{ins}$**. Assuming all collisions follow the lowest adiabatic triplet surface, a rate-determining entrance channel barrier ^{3}**TS$_{ent}$** (0.5−2 kcal/mol) to complex formation would then be necessary to limit the reaction efficiency, although no such barrier was found at the level of UB3LYP/LANL2DZ. Alternatively, nonadiabatic effects along the triplet entrance channel could also contribute to the reaction inefficiency. Some of the potentials emanating from the 5-fold electronically degenerate triplet ground-state Zr ($4d^25s^2$, $^3F_2$) + C_2H_4 are likely repulsive. Only a fraction of collisions may actually access the attractive adiabatic surface that leads to the formation of the metallacyclopropane complex and subsequent H_2 elimination.

We must now reassess these conclusions in light of the new theoretical results that have clearly identified three different reaction paths along two electronic spin surfaces. First, we consider the possibility that the Zr + ethylene reaction occurs *exclusively* on the adiabatic *triplet* PES. We repeated the RRKM calculations using the new UB3LYP/Stuttgart+6-311++G(d,p) rotational constants and vibrational frequencies for ^{3}**TS$_{ent}$**, ZrC_2H_4 ($^3A_2$) (**1b**), and ^{3}**TS$_{ins}$**. Because we find that the stationary point geometries and frequencies are relatively insensitive to the choice of basis set, neither the qualitative nor quantitative results of the earlier statistical model change. The calculated UB3LYP energy of ^{3}**TS$_{ent}$** (+0.78 kcal/mol) is consistent with the experimentally determined reaction efficiency. However, we must lower ^{3}**TS$_{ins}$** by 8 kcal/mol from the UB3LYP energy of +1.9 kcal/mol to −6.1 kcal/mol, much as before. Complexes then insert much faster than they dissociate, resulting in no isotope effect and no backscattered Zr at low collision energies; the centrifugal barrier atop ^{3}**TS$_{ins}$** scatters Zr back to reactants at the higher collision energies. The triplet PES then branches into two reaction paths from the insertion intermediate (**2b**), but the low-energy ^{3}**MCTS** ensures that the concerted mechanism dominates at all collision energies of interest here.

Statistical modeling of the kinetic energy release distributions is beyond the scope of this study, but qualitative comparison to the product scattering data suggests that neither triplet mechanism is consistent with the experimental distributions. The P(E_t') found to best fit the ZrC_2H_2 laboratory angular distribution at a collision energy of 14.0 kcal/mol peaks at 3−5 kcal/mol and extends to about 30 kcal/mol, indicating the presence of a small exit barrier. The UB3LYP exothermicity of −14.9 kcal/mol for triplet products compares favorably with the estimate of −16.0 kcal/mol from the maximum observed kinetic energy. However, along the lower energy concerted path, we find no exit barrier to elimination of H_2 from H_2−ZrC_2H_2 (**3b**). Even in the unlikely event that the 1 kcal/mol of potential energy at ^{3}**MCTS** is channeled entirely into translation, this triplet path cannot account for the product P(E_t') that peaks at 4 ± 1 kcal/mol. Along the higher energy stepwise path, the exit barrier ^{3}**TS$_{exit}$** lies 18 kcal/mol above products, which would almost surely result in a much larger kinetic energy release than observed experimentally.

2. Competitive Singlet Path. The present work raises the strong possibility that a significant fraction of the reactive events occur on the *singlet* PES. In this singlet mechanism, we assume that all reactive collisions first reach the triplet metallacyclopropane well (**1b**). Next, some fraction of the triplet complexes undergo triplet-to-singlet intersystem crossing (ISC) at a rate k_{ISC}, gaining access to the singlet metallacyclopropane well (**5**). The rate model for the triplet mechanism yields a rough bound on the time scale for which the spin transition must occur in order to compete with facile CH bond insertion on the triplet surface. With energies of ^{3}**TS$_{ent}$** (+0.78 kcal/mol) and ^{3}**TS$_{ins}$** (−6.1 kcal/mol) adjusted to fit the data as described above, the lifetime of triplet ZrC_2H_4 complexes with respect to CH bond insertion is about 1 ns at 300 K. Alternatively, in the extreme limit of no insertion on the triplet surface, ISC must be sufficiently fast (∼10 ns) so that no more than about 5% of triplet ZrC_2H_4 complexes dissociate back to reactants at low collision energy. In either event, ISC on a time scale of 1 ns or shorter would make the singlet mechanism competitive. Unfortunately, it is difficult to estimate a priori the absolute magnitude of k_{ISC}.[33]

If the singlet surface is reached, the present calculations indicate that subsequent H_2 elimination is also efficient, involving facile CH insertion by the metallacyclopropane (**5**) followed by stepwise rearrangement to the very deep dihydrido intermediate well (**7**). From RRKM calculations on the singlet surface, we find that even without downward adjustment the RB3LYP energy of −7.9 kcal/mol for ^{1}**TS$_{ins}$** is sufficiently low to account for the lack of a deuterium isotope effect and the absence of backscattered Zr at low collision energies. Rearrangement of the singlet insertion intermediate (**6**) to the dihydrido intermediate (**7**) is facile at all collision energies, since the barrier ^{1}**TS$_{\beta H}$** is so small. Reverse intersystem crossing from singlet $H_2ZrC_2H_2$ (**7**) back to the triplet surface is probably inefficient, since there is no triplet species with geometry or energy similar to **7**.

Therefore, we reason that those collisions that access the singlet surface are likely to eliminate H_2 from $H_2ZrC_2H_2$ (**7**) to produce the ZrC_2H_2 ($^1A_1$) + H_2 products. In fact, the small exit barrier ^{1}**TS$_{exit}$** (4 kcal/mol for RB3LYP) is more consistent with the peaking of the P(E_t') between 3 and 5 kcal/mol than is ^{3}**MCTS** or ^{3}**TS$_{exit}$** on the triplet surface. Although the calculated exothermicity of −8.3 kcal/mol for singlet products is smaller than the estimate of −16 kcal/mol from the experimental P(E_t'), the RB3LYP calculations likely underestimate the binding energy of ZrC_2H_2 ($^1A_1$) (**8**), and hence the exothermicity of singlet products. The spin-restricted method also overestimates the energy of ^{1}**TS$_{exit}$**. We emphasize that a more flexible open-shell singlet treatment would likely preserve the key ∼4 kcal/mol energy difference between ^{1}**TS$_{exit}$** and the ZrC_2H_2 ($^1A_1$) + H_2 product asymptote because the geometry of ^{1}**TS$_{exit}$** is already so product-like. Finally, in the singlet mechanism the data still require that a small approach barrier or nonadiabatic effects along the ground-state triplet entrance channel limit the reaction efficiency, as already described for the triplet mechanism.

3. Evidence from Different DFT Methods. Table 1 shows that for the triplet Zr + ethylene PES, the UB3LYP, U*m*PW1PW91, and UB1LYP functionals yield quite different energies at corresponding stationary points. Relative to reactants, the energies consistently lie in the order E(UB1LYP) > E(UB3LYP) > E(U*m*PW1PW91). At both transition states and potential wells, UB3LYP energies lie 2−4 kcal/mol below UB1LYP energies and U*m*PW1PW91 energies lie an *additional* 4−11 kcal/mol below UB3LYP energies. Similarly, Table 3 shows that the R*m*PW1PW91 energies are also lower by 5−7 kcal/mol than the corresponding RB3LYP energies for most stationary points along the singlet PES.

Ideally, we would use our statistical rate model to indicate the acceptable range of key stationary point energies based on

experimental data and thus help judge the accuracy of the different DFT methods. However, in the Zr + ethylene reaction the additional mechanistic possibilities introduced by discovery of the low-lying singlet surface make it very difficult to choose a preferred functional. Nevertheless, much experience has been garnered concerning the performance of the different functionals on other related systems. Based on the results of this study, it is clear that if the reaction took place entirely on the triplet PES, the rate-limiting ^{3}**TS$_{ins}$** must lie 4−7 kcal/mol below reactants, i.e., the UB3LYP energy must be lowered by 6−9 kcal/mol. This is only slightly more than the downward adjustments of 5−7 kcal/mol systematically required of rate-limiting multi-center transition states in analogous B3LYP studies of Co^+ and Ni^+ reactions with alkanes.[1−3,5] The UB1LYP energies are unrealistically high.

In contrast, the U*m*PW1PW91 energies seem quite consistent with experiment, predicting facile CH bond insertion on both the triplet and singlet surfaces. While placement of ^{1}**TS$_{ins}$** at −15.3 kcal/mol precludes any backscattering of Zr once reactants reach the singlet surface, placement of ^{3}**TS$_{ins}$** at −6.2 kcal/mol is consistent with the onset of backscattering of high angular momentum components for collision energy between 6 and 9 kcal/mol. Since the ISC rate remains unknown, the U*m*PW1PW91 energies do not answer the question of triplet/singlet branching. However, additional support for U*m*PW1PW91 energetics over UB3LYP energetics comes from our ongoing study of the simpler Y + ethylene reaction.[34] In that system, only a doublet electronic surface is important, allowing a more critical comparison of theory with experiment. For Y + C_2H_4, the UB3LYP functional again predicts CH bond insertion to be rate-determining, but places ^{2}**TS$_{ins}$** at +4.8 kcal/mol. RRKM calculations indicate that again we must lower the UB3LYP value by 6−9 kcal/mol to reproduce the experimental observations of a small positive isotope effect and a small fraction of stabilized YC_2D_4 collision complexes. In contrast, the U*m*PW1PW91 functional places ^{2}**TS$_{ins}$** at −3.0 kcal/mol, in good agreement with the chemical kinetics data.

Returning to Zr + ethylene, another difficult issue is the cause of the reaction inefficiency. Either a small entrance channel barrier exists, or a substantial fraction of collisions access repulsive excited-states at long range and fail to convert to the attractive potential leading to the triplet metallacyclopropane well (nonadiabatic effects). In the former picture, RRKM modeling requires that the ^{3}**TS$_{ent}$** barrier height be about 1 kcal/mol, in excellent agreement with the values of 0.8 and 1.2 kcal/mol obtained by UB3LYP and UB1LYP, respectively. However, both B3LYP and B1LYP are known to poorly model long-range intermolecular forces, finding, for example, that the He_2 and Ne_2 dimers are unbound near their van der Waals minima.[11,20] The *m*PW1PW91 functional, which uses the same ratio of exact/DFT exchange as B1LYP, but different exchange (*m*PW) and correlation (PW91) functionals, was designed in part to improve the long-range behavior.[19,20]The fact that U*m*PW1PW91 finds *no* triplet entrance channel barrier then suggests that the inefficiency of the reaction is more likely due to nonadiabatic effects. This picture can also explain why Zr reacts nearly three times faster with propylene than with ethylene.[12,4] Driven by the larger density of rovibronic states, a larger fraction of Zr + C_3H_6 collisions can make the requisite nonradiative transition to the attractive adiabatic surface prior to scattering back to reactants.

4. Preferred Mechanism. Our best inferences for the Zr + ethylene reaction mechanism gleaned from the new theoretical results, the statistical rate modeling, and all of the experimental data are summarized in Figure 6. The two surfaces shown are the lowest energy, concerted triplet path and the stepwise singlet path described in detail above. The energetics along both paths are those predicted by the *m*PW1PW91 functional (Tables 1 and 3), since those results seem most realistic. Accordingly, in the triplet entrance channel we draw a barrierless, attractive surface and a representative repulsive surface to suggest that the 7% reaction efficiency measures the fraction of room-temperature Zr + ethylene collisions that access the attractive surface and reach the metallacyclopropane complex (**1b**). Along the triplet concerted path connecting the insertion intermediate (**2b**) to elimination products (**4b**), U*m*PW1PW91 actually lowers ^{3}**MCTS** *below* the ZrC_2H_2 ($^3A_2$) + H_2 asymptote, so we draw a monotonically rising energy path from **2b** to **4b**. From **1b**, the three rate constants in boxes represent the competition between CH insertion and subsequent H_2 elimination on the triplet surface (k_{ins}), dissociation back to triplet reactants (k_{diss}), and intersystem crossing to the singlet surface (k_{ISC}) and subsequent H_2 elimination.

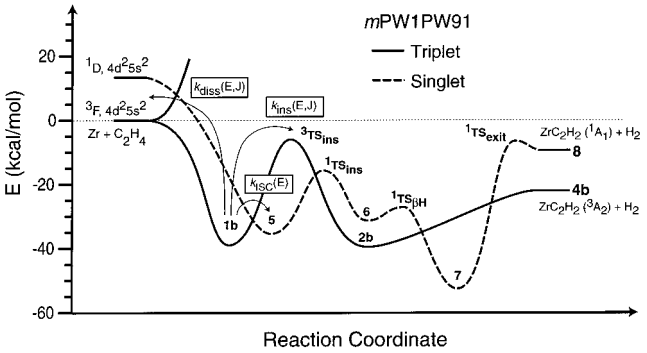

Figure 6. Schematic of lowest energy triplet and singlet reaction paths based on *m*PW1PW91 energetics, including three parallel, competitive decay rates from the triplet metallacyclopropane complex **1b**.

The outcome of this competition likely depends on both total internal energy E and complex angular momentum J. From RRKM theory, we expect $k_{ins}(E,J)$ to increase exponentially with E and to decrease rapidly with J (at fixed energy), since ^{3}**TS$_{ins}$** is a tight transition state. We expect $k_{diss}(E,J)$ to increase exponentially with E but to decrease more slowly with J, since the triplet entrance channel transition state is loose (little or no barrier). In contrast, from a wealth of experimental measurements of nonradiative transition rates, we expect k_{ISC} to increase only slowly with E and to be independent of J.[33] The reason is that the triplet complex (**1b**) and the singlet complex (**5**) have very similar geometries and electronic energies. Intersystem crossing rates in such near resonant cases can be very fast. For example, modest-sized ketones exhibit $S_1 \rightarrow T_1$ ISC rates of 10^9 s^{-1} or larger near the S_1 origin.[33] These rates increase roughly *linearly* with excess energy, presumably due to the modest electronic energy gap of ∼0.3 eV. By analogy, for the triplet ZrC_2H_4 complex (**1b**) we expect k_{ISC} to be fast, especially given the enhanced spin−orbit coupling in the 4d series. Ultimately, triplet-to-singlet ISC will compete with the rates k_{diss} and k_{ins} most effectively at low collision energy and for high-J complexes at higher collision energy.

The best experimental evidence for the singlet mechanism is the product kinetic energy distribution $P(E_t')$ obtained at reactant E_t = 14.0 kcal/mol. The distribution peaks between 3 and 5 kcal/mol, in accord with the calculated barrier on the singlet (but not the triplet) surface. If singlet elimination is competitive even at 14.0 kcal/mol, the singlet mechanism may well *dominate* in our 300 K kinetics experiments. While we cannot rule out

some contribution from the triplet mechanism, we expect that $P(E_t')$ on the triplet path would be statistical and peak very close to zero energy, in contrast to the experimental distribution. Assuming the R*m*PW1PW91 energy of −15.3 kcal/mol for ^{1}**TS$_{ins}$** is roughly correct, the rate model then indicates that the onset of backscattering of Zr at the higher collision energies cannot be due to reactants that reach the singlet surface. Rather, we suggest that at higher E_t the deflection of high-J complexes from ^{3}**TS$_{ins}$** on the *triplet* surface begins to overcome k_{ISC}, which increases only slowly with energy. Although the product kinetic energy distributions for reactant $E_t = 6-23$ kcal/mol show no evidence of bimodality, there may well exist an energy regime in which both triplet and singlet insertion mechanisms contribute to H_2 elimination products. Because the calculated singlet exit barrier is small and the calculated energy difference between singlet and triplet products is at most 10 kcal/mol, electronic branching may not be apparent in the broad $P(E_t')$ distributions observed.

V. Conclusions

This comprehensive theoretical study provides a detailed view of the Zr + ethylene reaction, including explicit characterization of all reaction intermediates along both the triplet and singlet spin surfaces. Along the triplet PES, we have identified a new lowest-energy path involving the concerted elimination of H_2, but *exclusive* reaction along this path appears to be inconsistent with the experimental data. Instead, we argue that primary CH insertion and stepwise H_2 elimination along the singlet PES must play an important role in explaining the behavior of Zr + ethylene, especially the product kinetic energy release. For the first time, a survey of the different DFT methods strongly suggests that the *m*PW1PW91 functional better represents the energies of transition metal species compared to the widely used B3LYP functional.

Despite this theoretical progress, additional experimental and computational work is needed to clarify the relative contributions of the triplet and singlet mechanisms as a function of reactant kinetic energy. Unfortunately, estimation of the key rate constant k_{ISC} is a difficult task.[33] Detailed modeling of the product kinetic energy distributions on both the triplet and singlet surfaces using phase space theory[32,35] at ^{3}**MCTS** and ^{1}**TS$_{exit}$** is now possible with the new electronic structure results as input. Product angular and kinetic energy distributions at lower collision energies would be more sensitive to the magnitude of small exit barriers and to product singlet−triplet branching. It also remains important to establish experimentally the existence or absence of an approach barrier, since this is a further distinguishing feature between *m*PW1PW91 and B3LYP. A study of the Zr + ethylene reaction using a variable-temperature flow reactor or a merged-beam apparatus at very low collision energies (<1 kcal/mol) would be quite revealing. Higher level, multi-configuration calculations of the singlet exit channel PES can greatly improve the description of the adiabatic singlet path and test whether the barrier ^{1}**TS$_{exit}$** remains substantial.

Similar theoretical and experimental studies of ground-state Y and Nb with ethylene and propylene are now in progress.[34,36] For Y, with only three valence electrons, we expect concerted H_2 elimination on the doublet surface to play an important mechanistic role. For Nb, much as for Zr, intersystem crossing from sextet reactants to the low-lying quartet surface is likely to be important. The goal of this work must be to place the entire collection of experimental and theoretical results for the reactions of Y, Zr, and Nb with alkenes within a comprehensive and consistent mechanistic picture.

We thank Prof. H. Floyd Davis for useful discussions. Generous support of this research has come from the National Science Foundation (Grants CHE-9616724 and NSF-0071458) and the donors of the Petroleum Research Fund (Grant 33441-AC6). M.P. thanks the UW-Madison Department of Chemistry for a Martha Weeks graduate fellowship.

Supporting Information Available: Rotational constants and vibrational frequencies of all stationary points calculated at the level UB3LYP/Stuttgart+6-311++G(d,p). Supporting Information is available free of charge via the Internet at http:///pubs.acs.org.

References and Notes

(1) Yi, S. S.; Blomberg, M. R. A.; Siegbahn, P. E. M.; Weisshaar, J. C. *J. Phys. Chem. A* **1998**, *102*, 395.

(2) Blomberg, M. R. A.; Siegbahn, P. E. M.; Yi, S. S.; Noll, R. J.; Weisshaar, J. C. *J. Phys. Chem. A* **1999**, *103*, 7254.

(3) Reichert, E. L.; Yi, S. S.; Weisshaar, J. C. *Int. J. Mass Spectrom.* **2000**, *196*, 55.

(4) Porembski, M.; Weisshaar, J. C. *J. Phys. Chem. A* **2000**, *104*, 1524.

(5) Yi, S. S.; Reichert, E. L.; Holthausen, M. C.; Koch, W.; Weisshaar, J. C. *Chem.-Eur. J.* **2000**, *6*, 2232.

(6) Holthausen, M. C.; Koch, W. *Helv. Chim. Acta* **1996**, *79*, 1939.

(7) Holthausen, M. C.; Fiedler, A.; Schwarz, H.; Koch, W. *J. Phys. Chem.* **1996**, *100*, 6236.

(8) Holthausen, M. C.; Koch, W. *J. Am. Chem. Soc.* **1996**, *118*, 9932.

(9) Becke, A. D. *J. Chem. Phys.* **1993**, *98*, 1372.

(10) Koch, W.; Hertwig, R. H. Density functional theory applications to transition metal problems. In *Encyclopedia of Computational Chemistry*; Schleyer, P., Ed.; John Wiley: New York, 1998; Vol. 1, p 689.

(11) Niu, S.; Hall, M. B. *Chem. Rev.* **2000**, *100*, 353.

(12) Carroll, J. J.; Haug, K. L.; Weisshaar, J. C. *J. Am. Chem. Soc.* **1993**, *115*, 6962.

(13) Carroll, J. J.; Haug, K. L.; Weisshaar, J. C.; Blomberg, M. R. A.; Siegbahn, P. E. M.; Svensson, M. *J. Phys. Chem.* **1995**, *99*, 13955.

(14) Wen, Y.; Porembski, M.; Ferrett, T. A.; Weisshaar, J. C. *J. Phys. Chem. A* **1998**, *102*, 8362.

(15) Willis, P. A.; Stauffer, H. U.; Hinrichs, R. Z.; Davis, H. F. *J. Phys. Chem. A* **1999**, *103*, 3706.

(16) Blomberg, M. R. A.; Siegbahn, P. E. M.; Svensson, M. *J. Phys. Chem.* **1992**, *96*, 9794.

(17) Siegbahn, P. E. M.; Blomberg, M. R. A.; Svensson, M. *J. Am. Chem. Soc.* **1993**, *115*, 1952.

(18) Siegbahn, P. E. M. *Theor. Chim. Acta* **1994**, *87*, 277.

(19) Adamo, C.; Barone, V. *Chem. Phys. Lett.* **1997**, *274*, 242.

(20) Adamo, C.; Barone, V. *J. Chem. Phys.* **1998**, *108*, 664.

(21) Andrae, D.; Haussermann, U.; Dolg, M.; Stoll, H.; Preuss, H. *Theor. Chim. Acta* **1990**, *77*, 123.

(22) Frisch, M. J.; Trucks, G. W.; Schlegel, H. B.; Scuseria, G. E.; Robb, M. A.; Cheeseman, J. R.; Zakrzewski, V. G.; Montgomery, J. A.; Stratmann, R. E.; Burant, J. C.; Dapprich, S.; Millam, J. M.; Daniels, A. D.; Kudin, K. N.; Strain, M. C.; Farkas, O.; Tomasi, J.; Barone, V.; Cossi, M.; Cammi, R.; Mennucci, B.; Pomelli, C.; Adamo, C.; Clifford, S.; Ochterski, J.; Petersson, G. A.; Ayala, P. Y.; Cui, Q.; Morokuma, K.; Malick, D. K.; Rabuck, A. D.; Raghavachari, K.; Foresman, J. B.; Cioslowski, J.; Ortiz, J. V.; Stefanov, B. B.; Liu, G.; Liashenko, A.; Piskorz, P.; Komaromi, I.; Gomperts, R.; Martin, R. L.; Fox, D. J.; Keith, T.; Al-Laham, M. A.; Peng, C. Y.; Nanayakkara, A.; Gonzalez, C.; Challacombe, M.; Gill, P. M. W.; Johnson, B.; Chen, W.; Wong, M. W.; Andres, J. L.; Head-Gordon, M.; Replogle, E. S.; Pople, J. A. *Gaussian 98*, Revision A.6; Gaussian, Inc.: Pittsburgh, PA, 1998.

(23) Koch, W.; Holthausen, M. C. *A chemist's guide to density functional theory*; Wiley-VCH: New York, 2000.

(24) Ziegler, T. *Chem. Rev.* **1991**, *91*, 651.

(25) Gill, P. M. W. Density functional theory (DFT), Hartree−Fock (HF), and the self-consistent field. In *Encyclopedia of Computational Chemistry*; Schleyer, P., Ed.; John Wiley: New York, 1998; Vol. 1, p 678.

(26) Hay, P. J. *J. Chem. Phys.* **1977**, *66*, 4377.

(27) Moore, C. E. *NBS Circ. No. 467*; U.S. Department of Commerce: Washington, DC, 1949; Vol. I−III.

(28) Glendening, E. D.; Badenhoop, J. K.; Reed, A. E.; Carpenter, J. E.; Weinhold, F. NBO 5.0, 5.0 ed.; Theoretical Chemistry Institute: University of Wisconsin, Madison, 1998.

(29) Schwenke, D. W.; Truhlar, D. G. *J. Chem. Phys.* **1985**, *82*, 2418.
(30) Carroll, J. J.; Weisshaar, J. C.; Siegbahn, P. E. M.; Wittborn, C. A. M.; Blomberg, M. R. A. *J. Phys. Chem.* **1995**, *99*, 14388.
(31) Gilbert, R. G.; Smith, S. C. *Theory of Unimolecular and Recombination Reactions*; Blackwell Scientific Publications: Oxford, U.K., 1990.
(32) Baer, T.; Hase, W. L. *Unimolecular reaction dynamics*; Oxford University Press: New York, 1996.
(33) Avouris, P.; Gelbart, W. M.; El-Sayed, M. A. *Chem. Rev.* **1977**, *77*, 793.
(34) Porembski, M.; Weisshaar, J. C. *J. Phys. Chem. A*, submitted.
(35) Hanratty, M. A.; Beauchamp, J. L.; Illies, A. J.; van Koppen, P. A. M.; Bowers, M. T. *J. Am. Chem. Soc.* **1988**, *110*, 1.
(36) Porembski, M.; Weisshaar, J. C. *J. Phys. Chem. A*, work in progress.